

Supplementary Information

Electrolyte Engineering Enables Rapid and Durable Zn— Air Self-charging Batteries

Jinghua Cai,^{a,b} Tao Li,^{a,b} Shicong Zhang,^{a,b} Xinji Dong,^{a,b} Tao Zhang,^{a,b} Yang Xu,^{a,b} Yi Shen,^{a,b} Chenyu

Wei,^{a,b} Hexian Ma,^{a,b} Fuqiang Huang,^{*a,b,c} and Tianquan Lin^{*a,b}

^a J. Cai, T. Li, S. Zhang, X. Dong, T. Zhang, Y. Xu, Y. Shen, C. Wei, H. Ma, F. Huang, T. Lin

Key Laboratory of Intelligent Creation for Extreme Energy Materials (MOE), School of Materials Science
and Engineering, Shanghai Jiao Tong University, Shanghai, 200240, P.R. China

Email: huangfq@sjtu.edu.cn; tqlin@sjtu.edu.cn

^b J. Cai, T. Li, S. Zhang, X. Dong, T. Zhang, Y. Xu, Y. Shen, C. Wei, H. Ma, F. Huang, T. Lin

Zhangjiang Institute for Advanced Study (ZIAS), Shanghai Jiao Tong University Shanghai 201210, P.R.
China

^c F. Huang

Inner Mongolia Research Institute, Shanghai Jiao Tong University, Hohhot 010010, China

Methods

Synthesis Method

(NH₄)₂V₁₀O₂₅·8H₂O nanobelts: (NH₄)₂V₁₀O₂₅·8H₂O nanobelts were prepared by a previous method.¹ Typically, 0.585 g NH₄VO₃ (99 %, Aladdin) and 0.63 g C₂H₂O₄·2H₂O (≥ 99.5 %, Aladdin) were added into 50 ml deionized water and stirred at room temperature for 1 h to obtain an orange solution. Finally, the above solution was transferred into a 100 mL Teflon-lined autoclave and heated at 180 °C for 3 h. After cooling to room temperature, the flocculent precipitates were washed with deionized water and dried at 60 °C.

(NH₄)₂V₁₀O₂₅·8H₂O@Pt nanobelts: (NH₄)₂V₁₀O₂₅·8H₂O @Pt nanobelts were prepared with a solution method. First, 0.1 g NVO nanobelts were added into 50 ml deionized water and ultrasonic 30 minutes. Second, 50 mg polyvinylpyrrolidone (PVP, Aladdin), 0.5 mg H₂PtCl₂·6H₂O (Pt 37.5% min, Macklin), and 40 ml methyl alcohol were added to the above solution. Then stir and ultrasonically this solution for 30 minutes at room temperature. Then, 0.1 mg mL⁻¹ NaBH₄ (98%, Aladdin) aqueous solvent was dropped in slowly. Finally, continue stirring for 1 h and then wash with deionized water, alcohol, and dried at 60 °C.

Solvothermal method to synthesis Zn_{x+y}(CF₃SO₃)_{2y}(OH)_{2x}·nH₂O crystal: 2 mol L⁻¹ Zn(CF₃SO₃)₂ (99 %, Aladdin) and 0.5 mol L⁻¹ KOH (≥99.5 %, Aladdin) were added into 20 mL N,N-Dimethylacetamide (DMAC, 90 vol%) and deionized water (10 vol%) mixture solvent stirred at room temperature for 30 minutes to obtain an clarifying solvent. Finally, the above solution was transferred into a 50 mL Teflon-lined autoclave and heated at 120 °C for 22 h. After cooling to room temperature, the flocculent precipitates were washed with deionized water and dried at 60 °C. In pure aqueous solvent as the same preparation and heating time only for 3h.

Characterization

The crystalline structure of NVO nanobelts and NVO@Pt interface was determined by powder X-ray diffractometer (XRD, Malvern Panalytical) with Cu Kα radiation (λ =

0.15405). The morphology and structure of the interface were characterized by scanning electron microscopy (SEM, Thermo Scientific Helios 5 CX) and transmission electron microscopy (TEM, FEI Talos F200X, and FEI Talos F200X G2) equipped with energy dispersive spectroscopy (EDS) for elemental analysis. The carbon nuclear magnetic resonance (^{13}C NMR) was collected using Nuclear Magnetic Resonance 500 (NMR 500). Fourier transform infrared spectroscopy (FT-IR, NICOLET 6700) and Raman spectroscopy (LabRAM Soleil, Horiba with excitation at 532nm) were collected to define the molecular structure. X-ray photoelectron spectroscopy (XPS) was collected by ESXCALAB Xi+ (Thermo Fisher Scientific). Time-of-flight-secondary ion mass spectroscopy (TOF-SIMS, Ion TOF ToF SIMS 5-100, Germany) was carried out to define the anion group in the degradation interface of NVO@Pt.

The desolvation energy of Zn^{2+} ions at DMAC and aqueous electrolytes, which were measured by the variation of Charge transfer resistance (R_{ct}) of $\text{Zn}||\text{Zn}$ batteries with the test temperature ranging from 30-70 °C, and calculated by the Arrhenius formula. The linear sweep voltammetry (LSV) of $\text{Zn}||\text{Ti}$ batteries was collected by using the CHI660E electrochemical workstation. The electrochemical performance of air self-charging and conventional $\text{Zn}||(\text{NH}_4)_2\text{V}_{10}\text{O}_{25}\cdot 8\text{H}_2\text{O}@Pt$ batteries was measured in an open fabricated battery and the CR2016 coin cell, respectively. The galvanostatic discharge/charging (GCD) tests were conducted by using a battery test system (LAND CT2001A) in a voltage range of 0.2-1.6 V.

Electrochemical measurement

Electrochemical performance of the $\text{Zn}||(\text{NH}_4)_2\text{V}_{10}\text{O}_{25}\cdot 8\text{H}_2\text{O}@Pt$ air self-charging battery was measured in an open-fabricated battery. The NVO@Pt electrode was prepared by mixing the above powder with MWCNT and PVDF in a weight ratio of 7:2:1 added into an appropriate amount NMP solvent, and stirred for 12 h. Then, the slurry was coated on titanium meshes and dried at 70 °C for 12 h under vacuum. The mass loading of NVO@Pt in the electrode is $\sim 1 \text{ mg cm}^{-2}$, (according to ICP-MS result (V: 39%, Pt: 0.4%), Pt mass is neglected). DMAC solvent with 10 vol% H_2O and 2 M $\text{Zn}(\text{CF}_3\text{SO}_3)_2$ zinc salt was adopted as DMAC electrolyte. In H_2O electrolyte was added

the same 2 M $\text{Zn}(\text{CF}_3\text{SO}_3)_2$ zinc salt. These open system batteries were assembled with the as-obtained NVO@Pt and Zn foil with a thickness of 30 μm as cathode and anode, respectively, in a glass bottle with 1 mL electrolyte and Ti electrode clamp. The coin cell was measured in CR2016, and commercial glass fiber and Zn foil with a thickness of 30 μm as the separator and anode, respectively. The galvanostatic discharge tests were carried out by using a battery test system (LAND CT2001A) in a voltage range of 0.2-1.6 V. The LAND system only records the battery voltage change when the battery is cycled through the air self-charging process. At O_2 atmosphere, 99.9% pure oxygen is slightly injected below the DMAC electrolyte level during the self-charging process.

Theoretical Calculation

The geometry optimization and density functional theory (DFT) chemical description for the molecular structures of all title compounds were performed using Gaussian 09 program² package with M062X exchange-correlation functional and 6-311+G** basis set^{3, 4} for C, H, O, N atoms and SDD for Zn atom. Harmonic vibration frequency calculations were performed for all stationary points to confirm them as a local minima (zero imaginary frequencies). Orbital composition, excited state analysis employed by Multiwfn program and VMD.^{5, 6} Approximate solvent effects were taken into consideration based on SMD (Solvation Model Based on Density) in all calculations.

Video illustration

The non-flammability of the DMAC-based electrolyte was confirmed by a comparative ignition test using glass fiber C separators soaked in either DMAC-based or H_2O electrolyte. Since the electrolyte consists of 90 vol% DMAC (boiling point: 165 °C, flash point: 70 °C) and 10 vol% non-flammable water, both separators failed to ignite within 3–4 s of exposure to a lighter flame. Although DMAC alone is flammable, the incorporation of 10 vol% H_2O effectively enhances the flame-retardant properties of the electrolyte. The experimental procedure and results are documented in Supplementary **Video S1**.

Table S1 Under identical conditions of temperature and air exposure, the mass data of 3 mL DMAC-based electrolyte and H₂O electrolyte were collected.

Electrolyte	Pristine	After 1 day	After 3 days	After 5 days	After 10 days
	(g)	(g)	(g)	(g)	(g)
DMAC	4.087	4.085	4.082	4.080	4.071
H ₂ O	4.062	4.026	3.946	3.861	3.656

Comparative evaporation tests were conducted under the same temperature and air exposure conditions as those used in the self-charging battery experiments. The mass changes of 3 mL samples of DMAC-based and H₂O electrolytes were recorded after 1, 3, 5, and 10 days. Owing to the much lower saturated vapor pressure of DMAC (0.17 kPa at 25 °C) compared to H₂O (3.17 kPa at 25 °C), the DMAC-based electrolyte exhibited significantly higher evaporation resistance (Table S1). Specifically, the average daily mass loss was only 0.4 % for the DMAC-based electrolyte, in contrast to 9.9 % for the H₂O electrolyte.

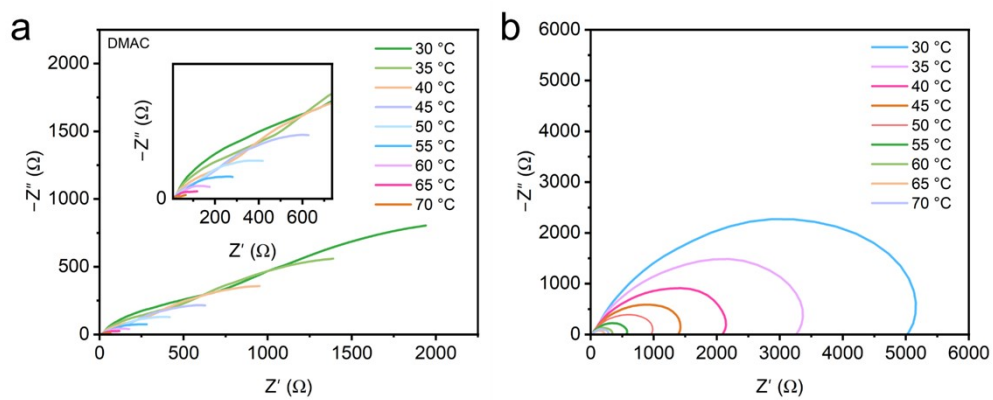
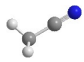
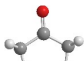
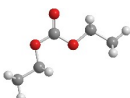
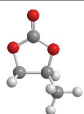
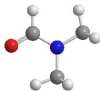
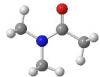
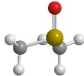




Fig. S1 EIS of Zn||Zn battery with DMAC-based and H₂O electrolyte at different temperatures from 70 °C to 30 °C.

Table S2 The relevant physicochemical parameters of the seven solvents.^{7, 8}

Solvent name	3D model diagram	DN	Saturated vapor pressure (mmHg, at 25 °C)	Flash point (°C, closed cup)
Acetonitrile (AN)		14	88.8	12.8
Acetone (ACE)		17	231	-16.99
Diethyl carbonate (DEC)		16	4.07 (Air = 1)	25
Propylene carbonate (PC)		15	0.045	135
N,N-dimethylformamide (DMF)		26.6	2.51 (Air = 1)	58
N,N-dimethylacetamide (DMAC)		27.8	2	70
Dimethyl sulfoxide (DMSO)		29.8	0.6	95 (open cup)
Pyridine (Py)		33.1	20.8	20
H ₂ O		18	23.75	/

i. Donor number of solvents is provided by Refs. 7-8.

ii. Saturated vapor pressure and flash point provided by the website of PubChem.

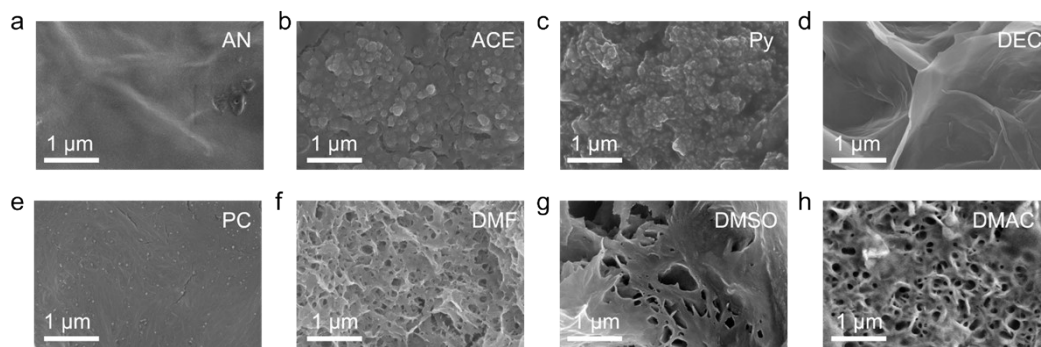


Fig. S2 SEM images of the cathode surface in the different electrolytes (containing 10 vol% H₂O and 0.5 M Zn(CF₃SO₃)₂). (a) Acetonitrile (AN). (b) Acetone (ACE). (c) Pyridine (Py). (d) Diethyl carbonate (DEC). (e) Propylene carbonate (PC). (f) N,N-dimethylformamide (DMF). (g) Dimethyl sulfoxide (DMSO). (h) N,N-dimethylacetamide (DMAC).

Although DMF also formed a porous interface, it suffered from gradual decomposition during cycling due to poor stability against reactive oxygen species.^{9,10}

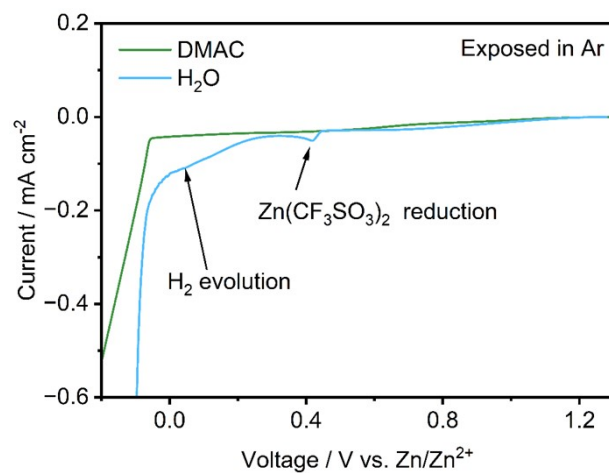


Fig. S3 LSV of DMAC and H₂O electrolyte in Zn||Ti batteries, which were exposed in an Ar environment.

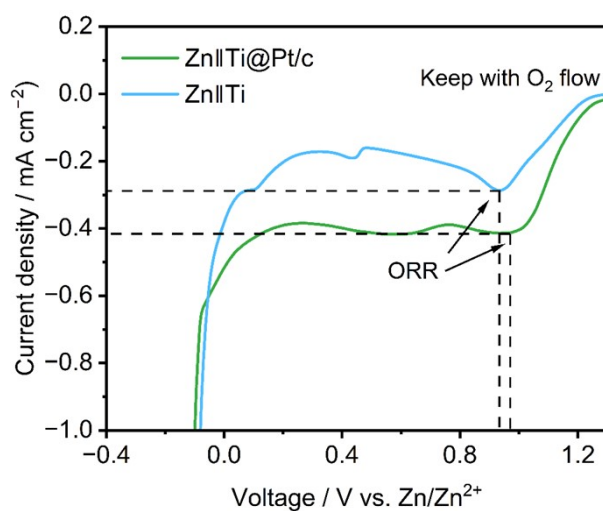


Fig. S4 The comparison of ORR in H₂O electrolytes under O₂ flow and scanned at 0.5 mV s⁻¹, which were tested by Zn||Ti and Zn||Ti@Pt batteries, respectively.

Ti@Pt/C was used as the working electrode (Zn as the counter electrode), the ORR peak exhibited a positive potential shift accompanied by a larger current density, consistent with the enhanced catalytic activity of Pt/C toward oxygen reduction.

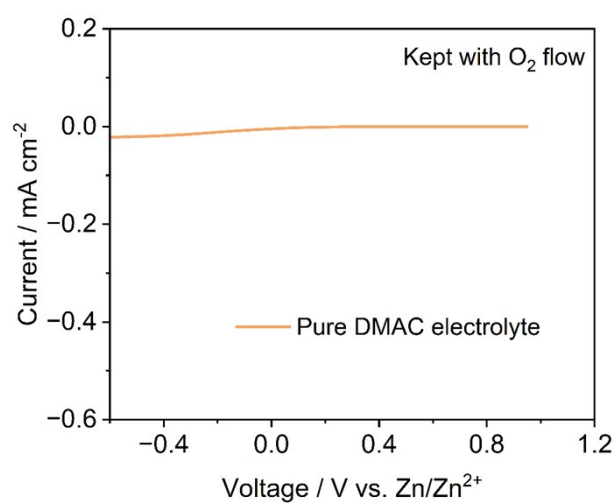


Fig. S5 LSV of pure DMAC electrolyte, which was kept with O₂ flow and scanned at 0.5 mV s⁻¹.

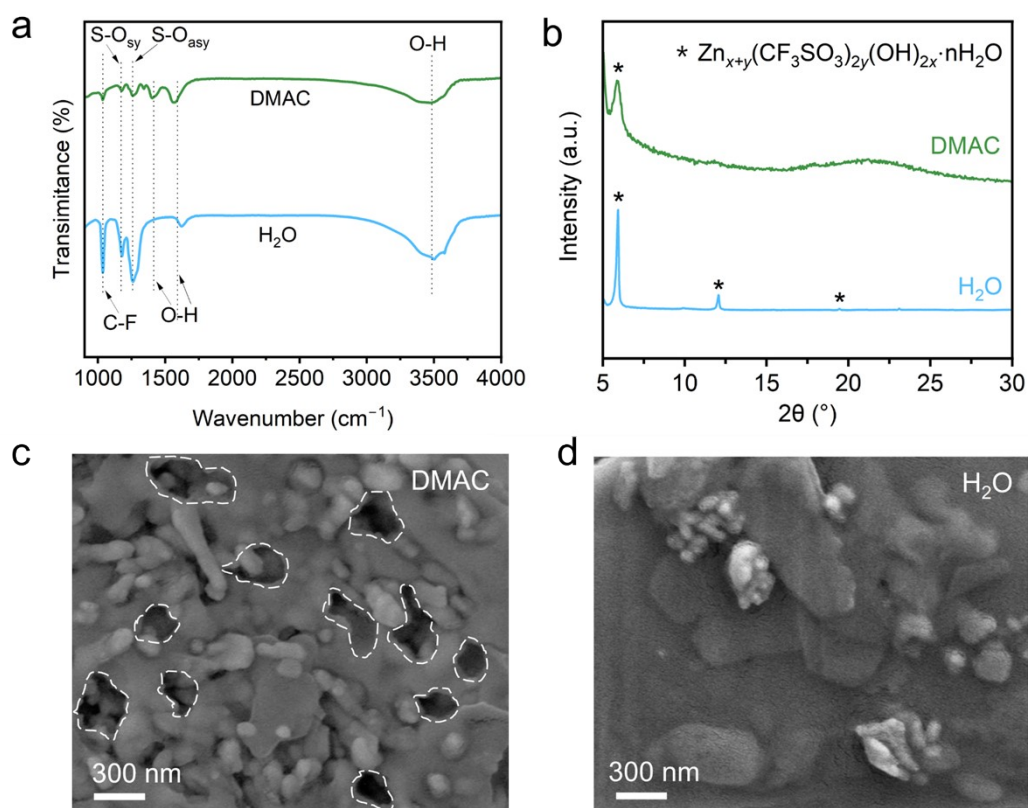


Fig. S6 (a) FT-IR spectra, (b) XRD patterns, (c) and (d) SEM images of solvothermal synthetic results comparison for the passivation particles ($\text{Zn}_{x+y}(\text{CF}_3\text{SO}_3)_{2y}(\text{OH})_{2x} \cdot n\text{H}_2\text{O}$) combining in DMAC and H₂O electrolytes, respectively.

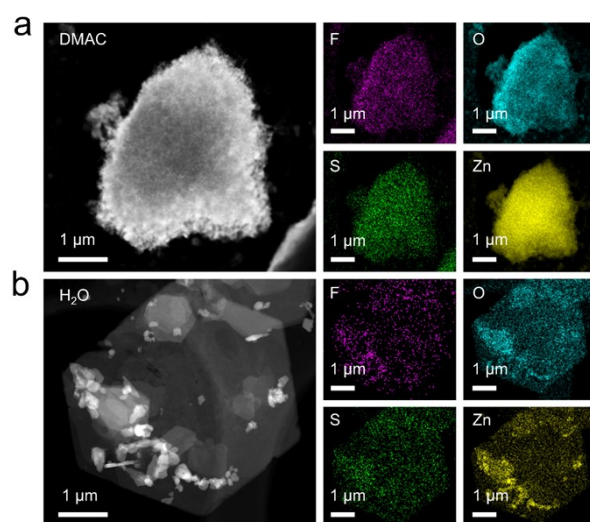


Fig. S7 High-angle annular dark field (HADDF) and the corresponding TEM-EDS elemental mapping images of $\text{Zn}_{x+y}(\text{CF}_3\text{SO}_3)_{2y}(\text{OH})_{2x} \cdot n\text{H}_2\text{O}$ crystal obtained from the solvothermal method of (a) DMAC-based and (b) H_2O electrolytes.

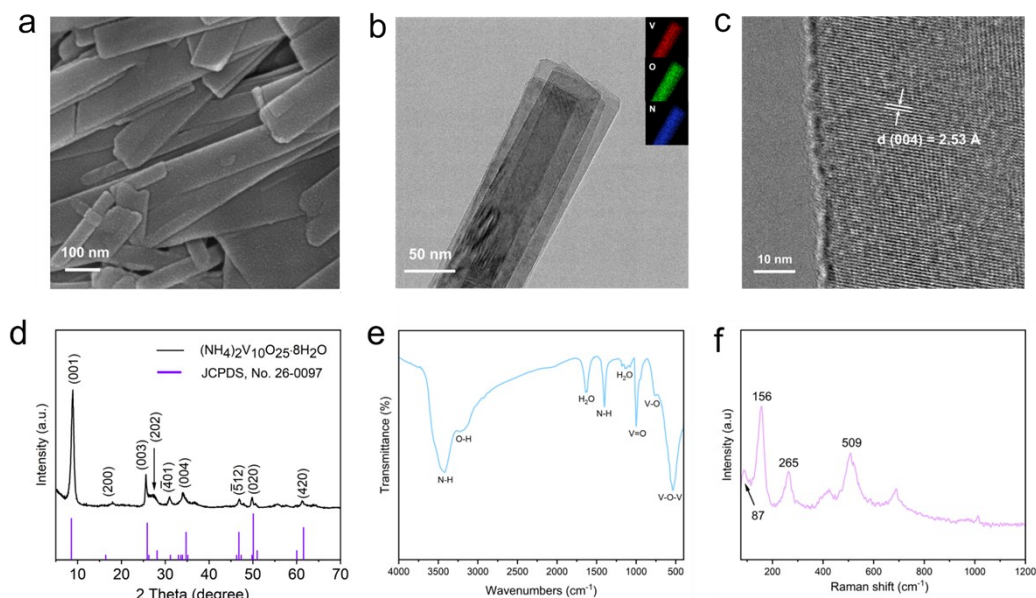


Fig. S8 Morphology and crystal structure of NVO nanobelt. (a) SEM image. (b) TEM image and the insert are the elemental mapping. (c) HRTEM image. (d) XRD pattern. (e) FT-IR spectra. (f) Raman spectra.

The $(\text{NH}_4)_2\text{V}_{10}\text{O}_{25}\cdot 8\text{H}_2\text{O}$ cathode was synthesized using a one-step hydrothermal method (see the synthesis method). X-ray diffraction (XRD) pattern presented in Fig. S8d, in which the diffraction peaks can be well indexed to the monoclinic NVO phase (JCPDS 26-0097) with lattice constants $a = 1.154$, $b = 0.364$, $c = 1.112$ nm, and $\beta = 112^\circ$. SEM and TEM images (Fig S8a and b) show that the nanobelt NVO is about 50~100 nm wide, and long for several micrometers. As shown in the HRTEM (Fig. S8c), the lattice fringe with a spacing of 2.53 Å is consistent with the (-310) lattice plane of NVO. To further confirm the structure of the prepared material, FT-IR and Raman spectroscopy are shown in Fig. S8e and f.

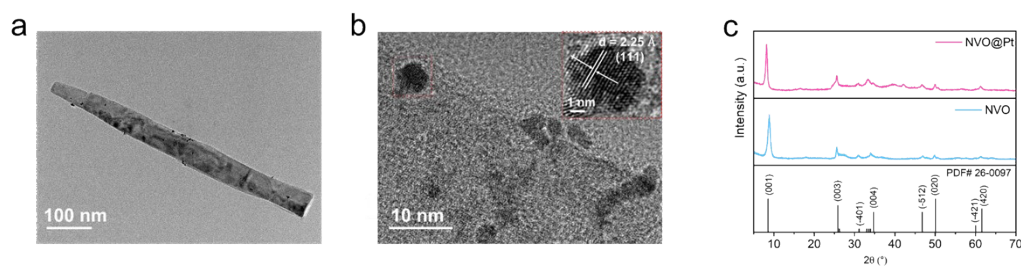


Fig. S9 Nanocrystals Pt are in-situ loaded on NVO surface as the oxygen reduction catalyst: (a) TEM image of the Pt nanocrystals loaded onto the $(\text{NH}_4)_2\text{V}_{10}\text{O}_{25}\cdot 8\text{H}_2\text{O}$ nanobelt surface.¹¹ (b) HRTEM image of $(\text{NH}_4)_2\text{V}_{10}\text{O}_{25}\cdot 8\text{H}_2\text{O}@\text{Pt}$, and the Pt high crystallinity image, the inset image is the Pt nanocrystals (111) lattice fringes with a d-spacing of 2.25 Å. (c) XRD patterns of $(\text{NH}_4)_2\text{V}_{10}\text{O}_{25}\cdot 8\text{H}_2\text{O}$ nanobelt (NVO) and Pt nanocrystals loaded onto the NVO nanobelt (NVO@Pt).

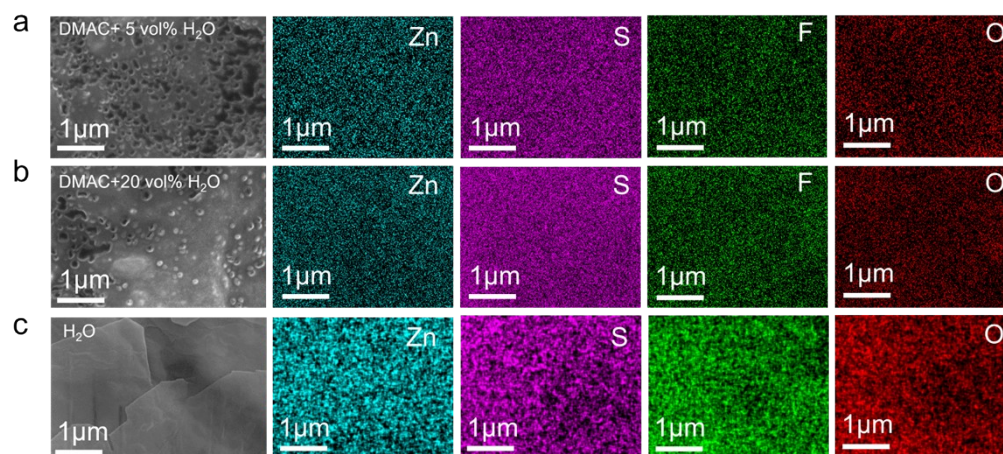


Fig. S10 SEM and the corresponding EDS images of NVO@Pt cathode interface after 20 cycles in DMAC-based electrolytes containing (a) 5 vol% H₂O, (b) 20 vol% H₂O, and (c) pure H₂O electrolyte, respectively.

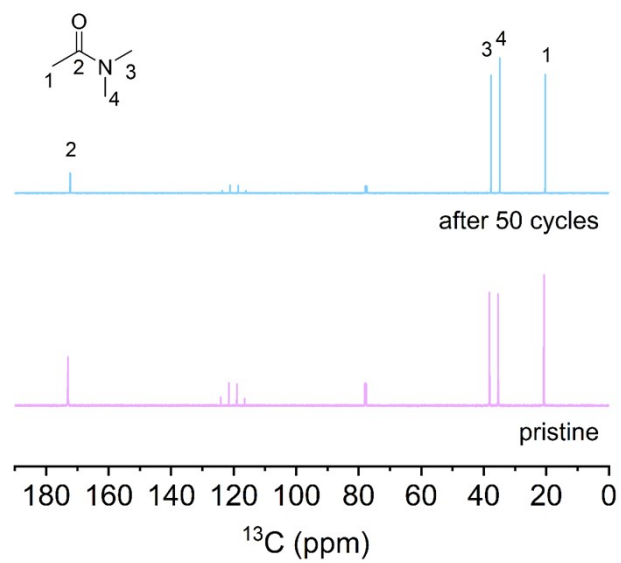


Fig. S11 Comparison of the ^{13}C spectra of the pristine DMAC-based electrolyte and after 50 cycles.

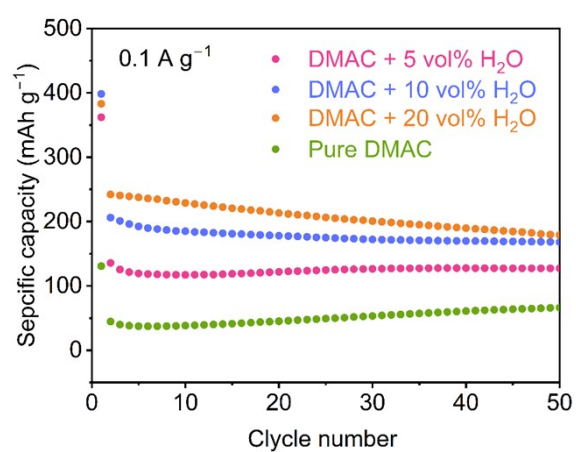


Fig. S12 The discharge capacity of Zn||NVO@Pt conventional batteries at 0.1 A g⁻¹ in different volumes of H₂O added in DMAC-based electrolytes.

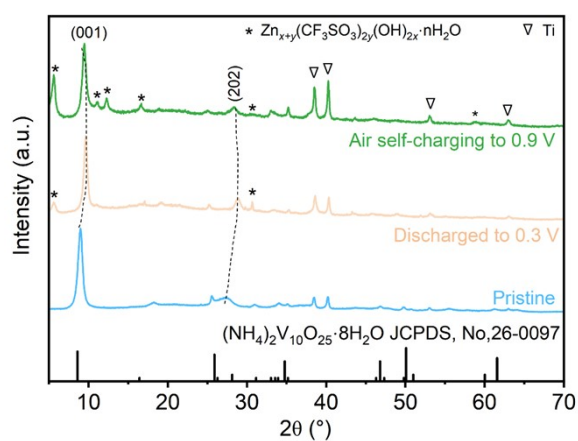


Fig. S13 XRD patterns of the NVO@Pt cathode collected at the pristine state, discharged to 0.3 V, and air self-charging to 0.9 V in DMAC-based air self-charging batteries.

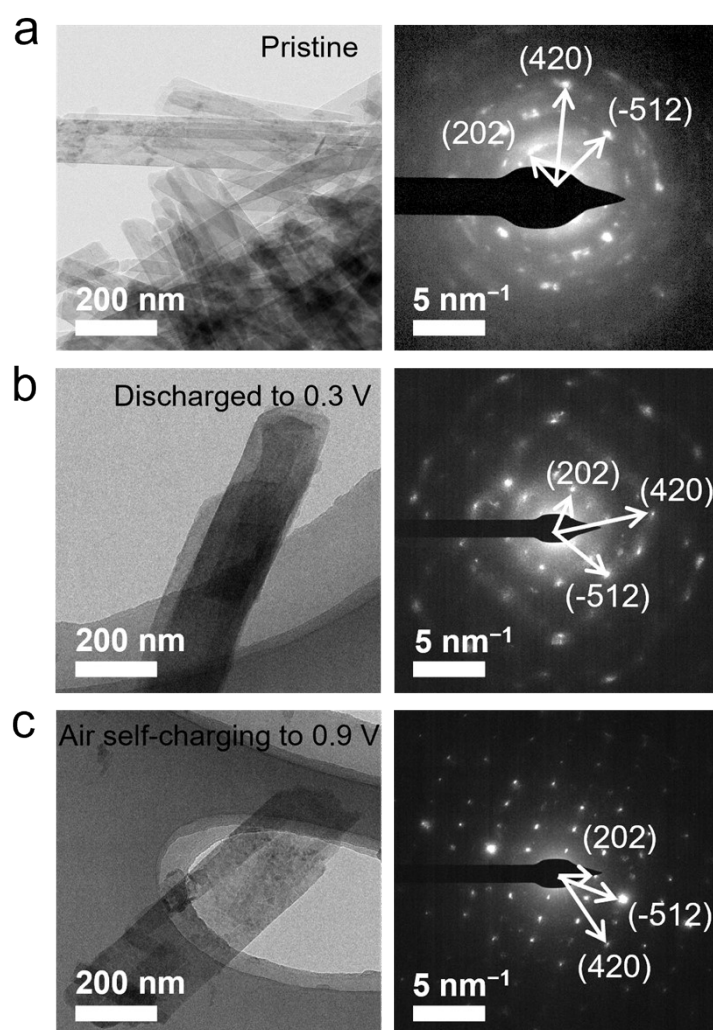


Fig. S14 TEM images and selected area electron diffraction of the NVO@Pt cathode, which were collected at the (a) pristine state, (b) discharged to 0.3 V, and (c) air self-charging to 0.9 V in DMAC-based air self-charging batteries.

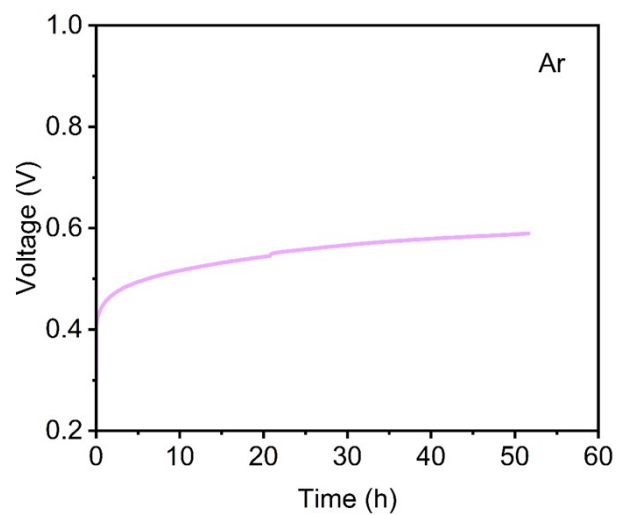


Fig. S15 The open circuit voltage changes of Zn||NVO@Pt self-charging battery in the Ar environment.

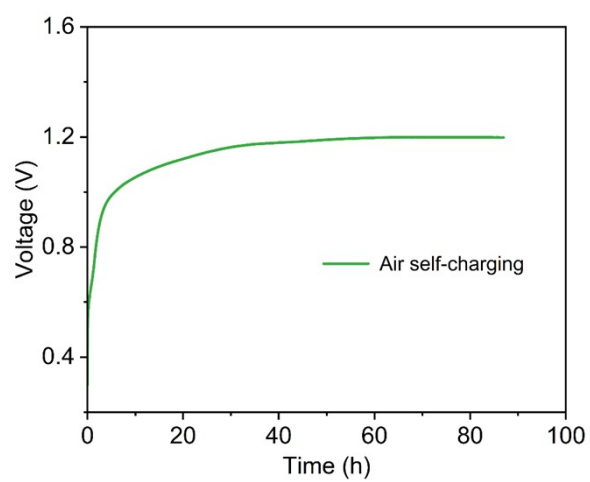


Fig. S16 The limited self-charging voltage of the Zn||NVO@Pt battery in the DMAC-based electrolyte, which was exposed to air.

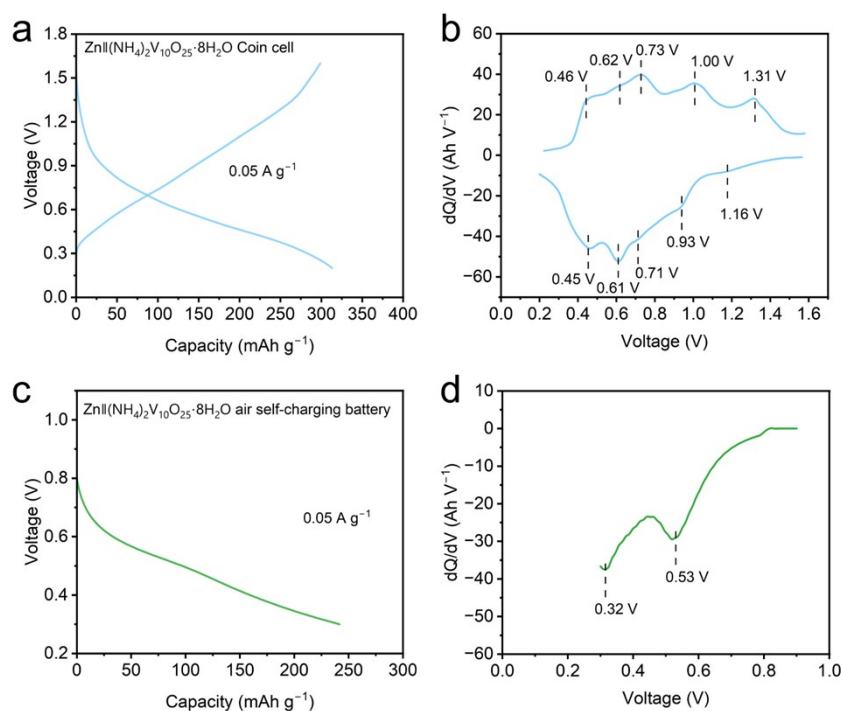


Fig. S17 (a) Galvanostatic charge/discharge profiles of Zn||NVO@Pt conventional cells at 0.05 A g⁻¹ in DMAC-based electrolyte, and (b) the corresponding dQ/dV curve. (c) Galvanostatic discharge profile of Zn||NVO@Pt air self-charging batteries at 0.05 A g⁻¹ in DMAC-based electrolyte, and (d) the corresponding dQ/dV curve.

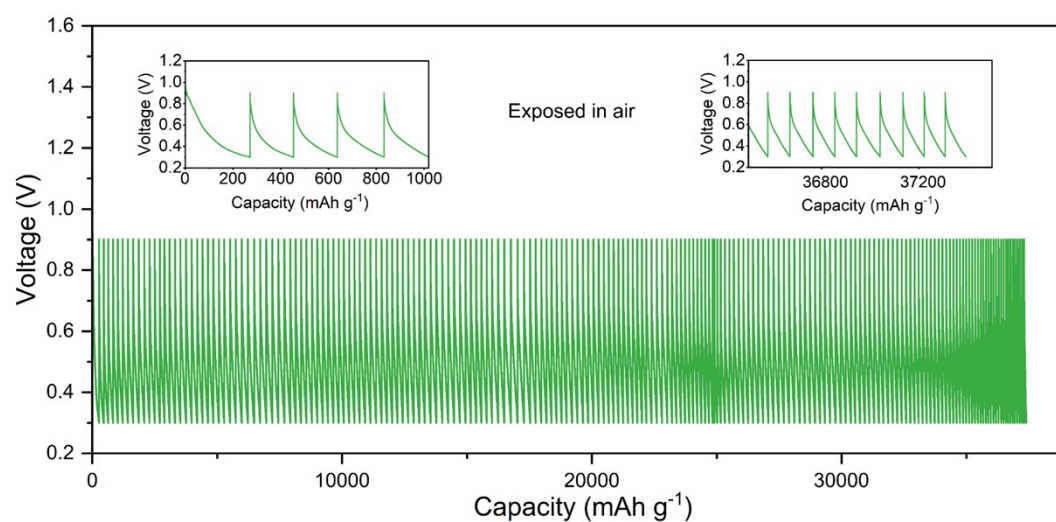


Fig. S18 Repeated air self-charging/galvanostatic discharge cycles of Zn||NVO@Pt air self-charging battery in DMAC-based electrolyte.

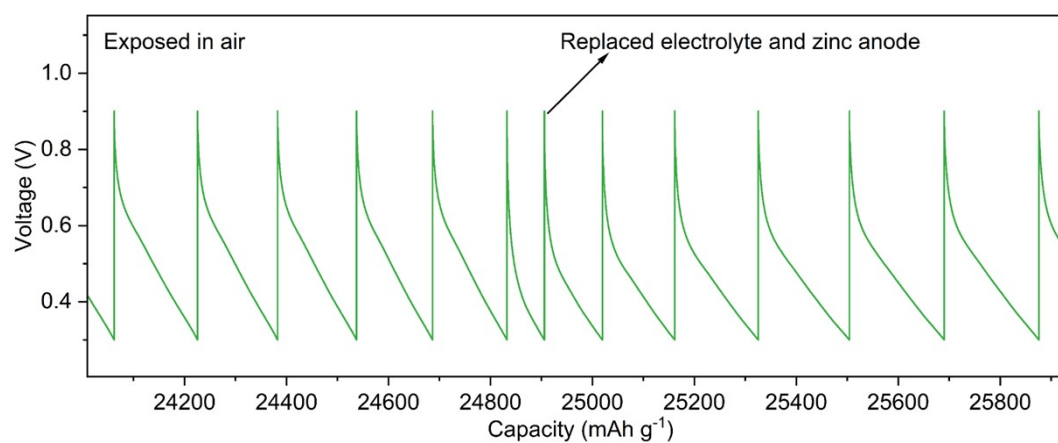


Fig. S19 The enlarged image of the repeated air self-charging/galvanostatic discharging cycles of the Zn||NVO@Pt battery when the DMAC-based electrolyte and zinc anode are replaced.

Table S3 The air self-charging capability and long cycle-life performance of the air self-charging batteries that have been reported until now.

Battery	Electrolyte	Air self-charging time	Cycle number	Current density (A g ⁻¹)	Capacity accumulation (mAh g ⁻¹)
Zn VS ₂ ¹²	2 M Zn(CF ₃ SO ₃) ₂	4.1 h to 0.9 V	4	0.2	1500
Zn PANI@Pt ¹¹	1 M Zn(CF ₃ SO ₃) ₂	9 h to 1.25 V	10	0.05	2180.8
Zn poly(4-HDPA)/AC ¹³	2 M Zn(CF ₃ SO ₃) ₂	12 h to 1.2 V	13	0.5	/
Zn CaVO ¹⁴	4 M Zn(CF ₃ SO ₃) ₂	24 h to 1.1 V	5	0.1	870
Zn AZPY ¹⁵	1 M ZnSO ₄	9 h to 1.1 V	24	/	5100
Zn VO ₂ ¹⁶	PAM-ChNF gel 1 M Zn(CF ₃ SO ₃) ₂ + 0.5 M CH ₃ COOH	3 h to 1.2 V	20	0.2	4000
Zn MoS ₂ /PANI ¹⁷	PAM/PEG gel 2 M Zn(CF ₃ SO ₃) ₂	24 h to 1.2 V	50	0.5	14000
Zn COF-PTO ¹⁸	1 M Zn(CF ₃ SO ₃) ₂	2 h to 1.1 V	100	1	6000
Zn VO ₂ ¹⁹	ZnSO ₄ + ZnI ₂	29 h to 1.2 V	9	0.3	1600
Zn PANINA ²⁰	2 M ZnCl ₂ + 3 M NH ₄ Cl	/	3	1	470
Zn Bi-MnO ₂ ²¹	2 M ZnSO ₄ + 0.2 M MnSO ₄	0.5 h to 1.28 V	10	0.1	1372.8
PAF-305-6K/	2 M	4 h to 1.13 V	20		4399

/H ₂ O/O ₂ /Pt ²²	Zn(CF ₃ SO ₃) ₂ + 12 M KCF ₃ SO ₃ (Zn-K)				
Pb PTO ²³	1 M H ₂ SO ₄	12 h to 0.85 V	200	1	23092
Zn NT-COF ²⁴	2 M ZnSO ₄	1 h to 1.25 V	10	0.2	1100
Zn poly(1,5-NAPD) ²⁵	6 M KOH + 0.2 M Zn(CH ₃ COO) ₂	24 h to 1.2 V	100	0.2	16500
Zn BQPH ²⁶	2 M ZnSO ₄	12 h to 1.2 V	5	1	1200
Zn NVO@Pt	DMAC with 10 vol% H ₂ O + 2 M Zn(CF ₃ SO ₃) ₂	4 h to 0.9 V	200	0.1	37392

References

- 1 T. Wei, Q. Li, G. Yang and C. Wang, *J. Mater. Chem. A.*, 2018, **6**, 20402-20410.
- 2 D. P. Chong, *Can. J. Chem.*, 2018, **96**, 336-339.
- 3 C. Lee, W. Yang and R. G. Parr, *Physical Review. B.*, 1988, **37**, 785-789.
- 4 R. Ditchfield, W. J. Hehre and J. A. Pople, *The Journal of Chemical Physics.*, 1971, **54**, 724-728.
- 5 T. Lu and F. Chen, *J. Comput. Chem.*, 2011, **33**, 580-592.
- 6 T. Lu and Q. Chen, *Comput. Theor. Chem.*, 2021, **1200**, 1133249.
- 7 Y. Wang, H. Yang, T. Hu, N. Piao, F. Li and H.-M. Cheng, *Natl. Sci. Rev.*, 2025, **12**, nwaf100.
- 8 P. Zhou, Y. Xiang and K. Liu, *Energy Environ. Sci.*, 2024, **17**, 8057-8077.
- 9 Y. Chen, S. A. Freunberger, Z. Peng, F. Bardé and P. G. Bruce, *J. Am. Chem. Soc.*, 2012, **134**, 7952-7957.
- 10 J. Li, S. Ding, S. Zhang, W. Yan, Z.-F. Ma, X. Yuan, L. Mai and J. Zhang, *Energy Storage Mater.*, 2021, **43**, 97-119.
- 11 W. Su, Y. Zhang, H. Wang, M. Yang and Z. Niu, *Adv. Mater.*, 2023, **36**, 2308042.
- 12 T. Li, X. Dong, H. Yang, J. Zhang, R. Huang, Z. Lv, Y. Li, S. Zhang, F. Huang and T. Lin, *Energy Environ. Sci.*, 2025, **18**, 3169-3176.
- 13 Q. Xu, X. Zhang, X. Yuan, W. Zhang, Y. Li, Y. Zhang and J. Liu, *Adv. Energy Mater.*, 2024, **14**, 2303475.
- 14 Y. Zhang, F. Wan, S. Huang, S. Wang, Z. Niu and J. Chen, *Nat. Commun.*, 2020, **11**, 2199.
- 15 D. Du, Y. Chen, H. Zhang, J. Zhao, L. Jin, W. Ji, H. Huang and S. Pang, *Angew. Chem. Int. Ed.*, 2024, **63**, e202408292.
- 16 C. Liu, W. Xu, C. Mei, M. Li, W. Chen, S. Hong, W. Y. Kim, S. y. Lee and Q. Wu, *Adv. Energy Mater.*, 2021, **11**, 20039902.
- 17 J. Shi, K. Mao, Q. Zhang, Z. Liu, F. Long, L. Wen, Y. Hou, X. Li, Y. Ma, Y. Yue, L. Li, C. Zhi and Y. Gao, *Nano Micro Lett.*, 2023, **15**, 53.
- 18 L. Zhong, C. Wang, J. He, Z. Lin, X. Yang, R. Li, S. Zhan, L. Zhao, D. Wu, H. Chen, Z. Tang, C. Zhi and H. Lv, *Adv. Mater.*, 2024, **36**, 2314050.
- 19 M. Zhang, T. Hu, X. Wang, P. Chang, L. Pan, Z. Jin, H. Mei, L. Cheng and L. Zhang, *Energy Storage Mater.*, 2022, **51**, 465-475.
- 20 X. Xie, Z. Fang, M. Yang, F. Zhu and D. Yu, *Adv. Funct. Mater.*, 2021, **31**, 2007942.
- 21 J. Zhao, X. Ge, A. Kumar, K. Yan, Y. Sun, X. Liu, X. Li and J. Pan, *Energy Storage Mater.*, 2025, **80**, 104360.
- 22 J. Wang, X. Zhang, Z. Liu, J. Yu, H. G. Wang, X. L. Wu, F. Cui and G. Zhu, *Angew. Chem. Int. Ed.*, 2024, **63**, e202401559.
- 23 F. Yue, Z. Tie, Y. Zhang, S. Bi, Y. Wang and Z. Niu, *Angew. Chem. Int. Ed. Engl.*, 2022, **61**, e202208513.
- 24 L. Zhao, C. Zhu, J. Ji, M. Li, Z. Kou, W. Li, F. Cai and L. Yuan, *Energy Storage Mater.*, 2025, **78**, 104273.
- 25 L. Yan, Y. Zhang, Z. Ni, Y. Zhang, J. Xu, T. Kong, J. Huang, W. Li, J. Ma and Y. Wang, *J. Am. Chem. Soc.*, 2021, **143**, 15369-15377.
- 26 Z. Tie, Y. Zhang, J. Zhu, S. Bi and Z. Niu, *J. Am. Chem. Soc.*, 2022, **144**, 10301-10308.